Multi-Element Transmitter Design and Performance Evaluation for Visible Light Communication

Yusuf Said Eroglu†, Alphan Sahin†, Ismail Guvenc†, Nezih Pala†, and Murat Yuksel‡
†Department of Electrical and Computer Engineering, Florida International University, Miami, FL
‡Department of Computer Science and Engineering, University of Nevada, Reno, NV
Email: {yerog001,asahin,iguvenc,npala}@fiu.edu, yuksem@cse.unr.edu

***Abstract*—Visible light communication (VLC) systems have significant potential for enabling broadband data rates by relying on the existing lighting infrastructure. In this paper, we investigate the performance of a multi-element VLC transmitter architecture for different configurations. In particular, we consider multi-element transmitters with three, seven, and nineteen light emitting diodes (LEDs). For a fixed number of LEDs installed in a room, we evaluate the signal-to-interference-plus-noise ratio (SINR) distributions across the room considering different transmitter geometries and a multipath VLC environment. Illumination distributions in the room are also generated for different configurations, and performance trade-offs for different transmitter architectures are investigated. Impact of transmit power at the LEDs and field of view at VLC receivers on the SINR performance are explored. Simulation results show that transmitter configuration with three LED gives the best performance for simultaneously achieving good illumination and SINR distribution under different circumstances.**

***Index Terms*—Free space optics (FSO), illumination, multipath, optical wireless communication (OWC), visible light communications (VLC).**

I. Introduction

VLC is a promising wireless technology for next generation broadband communication [1], [2] and wireless localization systems [3], [4]. A distinct feature of the VLC technology is that it achieves communication and illumination at the same time and enables energy efficient communications using the existing lighting infrastructure. Effective design of VLC systems requires illumination, communication, and cost constraints to be simultaneously taken into account. For example, designing the system for homogeneous illumination may on the other hand increase the interference experienced by the VLC receivers. For the long-term success of VLC, it carries critical importance to have satisfactory communication and illumination in a cost-effective manner. In this paper we study different multi-element VLC transmitter architectures, and investigate favorable VLC deployment approaches to simultaneously achieve good communication and illumination.

Existing research on VLC systems is focused around increasing the field of view (FOV), communication range, and data rate, and they investigate improvements via single-element transmitter or receiver architectures. Some recent such studies in the literature study illumination and communication trade-offs [5]–[8]. In [9]–[12] multi-element VLC receivers are studied to improve reception performance. On the other hand, to the best knowledge of the authors, there are no existing studies in the literature specifically investigating illumination and communication design trade-offs for multi-element VLC transmitters. In [13], a hemispherical multi-element transmitter design is introduced and its hybrid usage with radio frequency communication is investigated. On the other hand, its efficiency is not compared to other transmitter schemes in terms of communication and illumination performance. Further, [13] did not consider multipath effects and just focused on a two-receiver case.

In this study, we investigate different VLC transmitter structures and discuss their impacts on SINR and illumination distributions. Four different transmitter models are studied. The first model includes a single-element transmitter which has one LED. When multiple single-element VLC transmitters are placed with short separation distance, high SINR and homogeneous illumination can be obtained. However, this increases the installation cost, as all the transmitters are needed to be individually installed on the ceilings and connected to electricity and network. In addition, the required circuit may increase the cost significantly. Other transmitter models involve three, seven, and nineteen LEDs, respectively.

We consider two different transmission schemes. In the first scheme, all the LEDs on the same transmitter transmit the same data. When the number of elements on a transmitter increases, it spans a wider area and provides higher SINR while reducing the cost. In the second scheme, all the LEDs transmit a different data stream, considering a multiuser communication scenario. In this second scenario, when the number of elements on a transmitter increases, the SINR is reduced, since neighbor elements cause interference. Using extensive simulations in a multipath environment, we investigate illumination and communication performance of VLC systems considering different transmission schemes and configurations. Impact of transmission power as well as the FOV at the VLC receiver are also explored.

The rest of this paper is organized as follows. Section II presents the VLC system model, while Section III introduces a novel method for efficient calculation of the channel impulse response in a multipath environment. Section IV explains the architecture of multi-element VLC transmitters and their SINR formulations. Section V provides simulation results considering various deployment scenarios, and the last section concludes the paper.

II. System Model

A. Deployment

We consider K visible light access points (VAPs) operating in the same spectrum and communicating with their own VLC

978-1-4673-9526-7/15/$31.00 ©2015 IEEE

receivers. Each VAP consists of M LEDs. The location of mth LED of kth VAP and its orientation are denoted by $\mathbf{r}_{mk} \in \mathbb{R}^{3\times 1}$ and $\mathbf{n}_{mk} \in \mathbb{R}^{3\times 1}$ in Cartesian coordinate system, respectively. We assume that the transmit powers of the LEDs are identical and denoted by P_0. Without loss of generality, we tag one of the VLC receivers. The location of the tagged VLC receiver and its orientation are denoted by $\mathbf{r}_{\mathrm{R}} \in \mathbb{R}^{3\times 1}$ and $\mathbf{n}_{\mathrm{R}} \in \mathbb{R}^{3\times 1}$, respectively.

B. Channel Model

Without loss of generality, a light source $\mathcal{S}$ can be characterized with three parameters as

$$\mathcal{S} = \{\mathbf{r}_{\mathrm{source}}, \mathbf{n}_{\mathrm{source}}, n\} \ , \tag{1}$$

where $\mathbf{r}_{\mathrm{source}} \in \mathbb{C}^{3\times 1}$ is the location of the light source, $\mathbf{n}_{\mathrm{source}} \in \mathbb{C}^{3\times 1}$ is the orientation of light source, and n is the parameter that specifies the directionality of the light source based on Lambertian pattern. A receiver $\mathcal{R}$ is modeled as

$$\mathcal{R} = \{\mathbf{r}_{\mathrm{receiver}}, \mathbf{n}_{\mathrm{receiver}}, A_{\mathrm{R}}, \theta_{\mathrm{FOV}}\} \ , \tag{2}$$

where $\mathbf{r}_{\mathrm{receiver}} \in \mathbb{C}^{3\times 1}$ is the location of the photo detector (PD), $\mathbf{n}_{\mathrm{receiver}} \in \mathbb{C}^{3\times 1}$ is the orientation of the PD, A_{R} is the area of PD in m^2, and θ_{FOV} is the FOV of PD.

1) LOS Impulse Response: In [14], the line-of-sight (LOS) component of the channel impulse response between the source $\mathcal{S}$ and the receiver $\mathcal{R}$ is given by

$$h^{(0)}(t;\mathcal{S},\mathcal{R}) = \frac{n+1}{2\pi}\cos^n(\phi)\cos(\theta)\frac{A_{\mathrm{R}}}{R^2} \times \Pi\left(\frac{\theta}{\theta_{\mathrm{FOV}}}\right)\Pi\left(\frac{\phi}{\pi/2}\right)\delta\left(t-\tau\right) \ , \tag{3}$$

where ϕ is the angle between the source orientation vector and the incidence vector, θ is the angle between the receiver orientation vector and the incidence vector, R is the distance between the source and the receiver, $\tau = R/\mathrm{c}$ is the propagation delay, c is the speed of light, $\delta(\cdot)$ is the Dirac function, and $\Pi(\cdot)$ is the rectangle function defined as

$$\Pi(x) \triangleq \begin{cases} 1 & \text{for } |x| \le 1 \\ 0 & \text{for } |x| > 1 \end{cases} \ . \tag{4}$$

The parameters of (3) can be obtained as

$$\cos(\phi) = \frac{\mathbf{n}_{\mathrm{source}}^{\mathrm{T}}(\mathbf{r}_{\mathrm{receiver}} - \mathbf{r}_{\mathrm{source}})}{R} \ , \tag{5}$$

$$\cos(\theta_{mk}) = -\frac{\mathbf{n}_{\mathrm{receiver}}^{\mathrm{T}}(\mathbf{r}_{\mathrm{receiver}} - \mathbf{r}_{\mathrm{source}})}{R_{mk}} \ , \tag{6}$$

and

$$R = \|\mathbf{r}_{\mathrm{receiver}} - \mathbf{r}_{\mathrm{source}}\|_2 \ . \tag{7}$$

While $\Pi(\theta/\theta_{\mathrm{FOV}})$ in (3) implies that the receiver can detect the light only when θ is less than θ_{FOV}, $\Pi(\phi/(\pi/2))$ ensures that the location of the receiver is in the FOV of the source.

2) NLOS Impulse Response: The non-line-of-sight (NLOS) components of the channel between an LED and a PD is obtained based on *multiple-bounce impulse response* model described in [14]. In this model, light from a source $\mathcal{S}$ can reach a receiver $\mathcal{R}$ after infinitely many number of diffuse reflections and the channel impulse response is expressed as

$$h(t;\mathcal{S},\mathcal{R}) = \sum_{d=0}^{\infty} h^{(d)}(t;\mathcal{S},\mathcal{R}) \ , \tag{8}$$

where t is the time index. Theoretically, $h^{(d)}(t;\mathcal{S},\mathcal{R})$ can be expressed as a recursive function given by

$$h^{(d)}(t;\mathcal{S},\mathcal{R}) = \int_S \rho_{\mathrm{ref}} \times h^{(0)}(t;\mathcal{S},\{\mathbf{r}_{\mathrm{ref}},\mathbf{n}_{\mathrm{ref}},\mathrm{d}A,\frac{\pi}{2}\}) * h^{(d-1)}(t;\{\mathbf{r}_{\mathrm{ref}},\mathbf{n}_{\mathrm{ref}},1\},\mathcal{R}), \tag{9}$$

where $*$ denotes the convolution operation. In (9), the vector $\mathbf{r}_{\mathrm{ref}} \in \mathbb{C}^{3\times 1}$ and the vector $\mathbf{n}_{\mathrm{ref}} \in \mathbb{C}^{3\times 1}$ correspond to the location and the orientation of the reflector, respectively, $\mathrm{d}A$ is the infinite decimal area of the reflector, and $\rho_{\mathrm{ref}} \in [0,1)$ is the reflection coefficient. In addition, the mode and the FOV of the reflector are set to 1 and $\pi/2$, respectively.

III. Efficient Calculation of Channel Response

In practice, the integration in (9) can be evaluated by using the method of Riemann summation. The summation can be further simplified by exploiting the recursive structure of (9). However, when the operations are applied in time domain, the proposed method in [14] may still be time consuming and limits the number of reflections taken into account for (8). In order to avoid this limitation, we calculate (9) based on channel frequency response and corresponding matrix formulation, which allows efficient calculation of (9) for any given reflection order.

Assume that N reflectors are taken into account in order to model the multipath channel in the environment. Such a spatial discretization leads to (9). Then, let $\mathbf{C}(f) \in \mathbb{R}^{(N+1)\times(N+1)}$ be a matrix where the entry at ith row and jth column is

$$\{\mathbf{C}(f)\}_{ij} = h^{(0)}(t;\mathcal{S}_j,\mathcal{R}_i)\exp(\mathrm{j}2\pi\tau_{ij}f) \ , \tag{10}$$

where i is the receiver index, j is the source index, $\mathcal{R}_i$ is the ith receiver, $\mathcal{S}_j$ is the jth source, and τ_{ij} is the propagation delay, and f is the frequency index. Without loss of generality, $\mathcal{R}_1$ and $\mathcal{S}_1$ are the parameter sets for the LED and the PD, respectively, and the reflectors are indexed by $i,j \in \{2,3,\ldots,N+1\}$. Then, the received signal components at the receiver and the reflectors due to the light experiencing exactly $d > 1$ bounces is obtained as

$$\mathbf{p}_d(f) = \left[\mathbf{C}(f)\mathbf{D}\right]^d \mathbf{p}_0(f) \ , \tag{11}$$

where $\mathbf{p}_d(f)$ is the received signal power due to the dth order reflections, $\mathbf{D}$ is a diagonal matrix where the diagonal elements include the reflection coefficients with entry $\{\mathbf{D}\}_{11}$ is set to 0, and the vector $\mathbf{p}_0(f)$ consists of the received signal power at the nodes due to the LOS component of the channel. The vector $\mathbf{p}_0(f)$ can be calculated as

$$\mathbf{p}_0(f) = \mathbf{C}(f)\mathbf{e} \ , \tag{12}$$

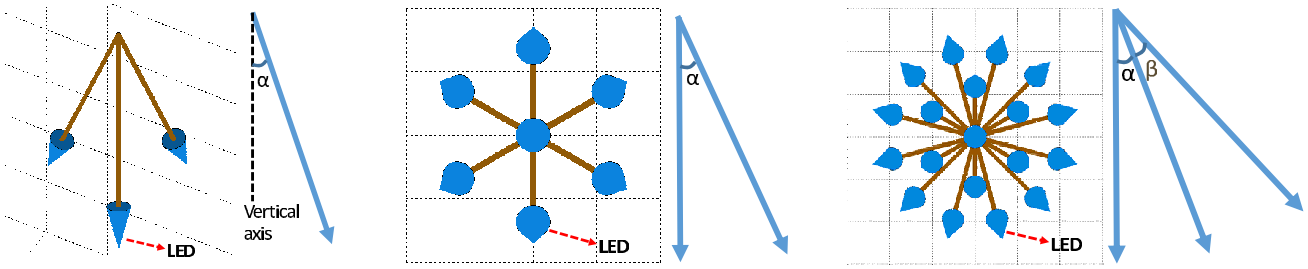

(a) 3-element transmitter architecture. (b) 7-element transmitter architecture. (c) 19-element transmitter architecture.

Fig. 1: Three different multi-element transmitter architectures that are considered. All transmitters are mounted on the ceiling, and all LEDs are facing down. Fig. 1(a) shows the side view of 3-element transmitter, while Fig. 1(b) and Fig. 1(c) are the top views of 7-element and 19-element transmitters, respectively.

where $\mathbf{e} \in \mathbb{R}^{(N+1)\times 1}$ is the excitation vector with the first entry is 1 and the rest of the entries are zeros.

By using the eigenvalue decomposition of $\mathbf{C}(f)\mathbf{D}$, (11) can be rewritten as

$$\mathbf{p}_d(f) = \mathbf{Q}\big[\mathbf{\Lambda}(f)\big]^d \mathbf{Q}^{-1}\mathbf{p}_0(f) \ , \tag{13}$$

where $\mathbf{Q} \in \mathbb{C}^{(N+1)\times(N+1)}$ is a matrix whose columns are the eigenvectors of $\mathbf{C}(f)\mathbf{D}$ and $\mathbf{\Lambda}$ is the diagonal matrix whose diagonal elements are the corresponding eigenvalues. Therefore, (11) can be calculated efficiently for an arbitrary number of multipath reflections, since $\mathbf{\Lambda}$ is a diagonal matrix. By evaluating (13) for different frequency, channel frequency response (CFR) can be calculated for a given bandwidth and one can calculate the CIR from CFR by using inverse Fourier transformation.

IV. Multi-Element VLC Transmitter Architectures

In this section, we present four different possible transmitter configurations and layouts, where the total number of LEDs in the room for each configuration is similar.

A. Transmitter Architectures and Room Layouts

Three of the four transmitter architectures considered in this paper are shown in Fig. 1. For the fourth architecture, we assume that there is a single LED at each transmitter. In the single LED transmitter configuration, all the LEDs are vertically directed downwards to the floor. In the 3-element transmitter configuration, LEDs have an angle α with the vertical axis, and each LED is separated with a horizontal angle of $120°$. In the 7-element transmitter configuration, one LED at the center is directed downwards, with a second layer of six LEDs uniformly placed around it. These six LEDs are positioned with a vertical angle α from the center LED. Finally, in the 19-element transmitter scenario, an LED at the center is directed downwards, and it is surrounded by two layers of LEDs around it. There are six LEDs in the first layer, and twelve LEDs in the second layer, vertically separated from the center LED by an angle of α and $\alpha + \beta$, respectively. Deployment layouts for all these four LED transmitter architectures are shown in Fig. 2.

B. SINR Calculations

Given the configuration, we consider two particular scenarios for capturing the SINR statistics within the room.

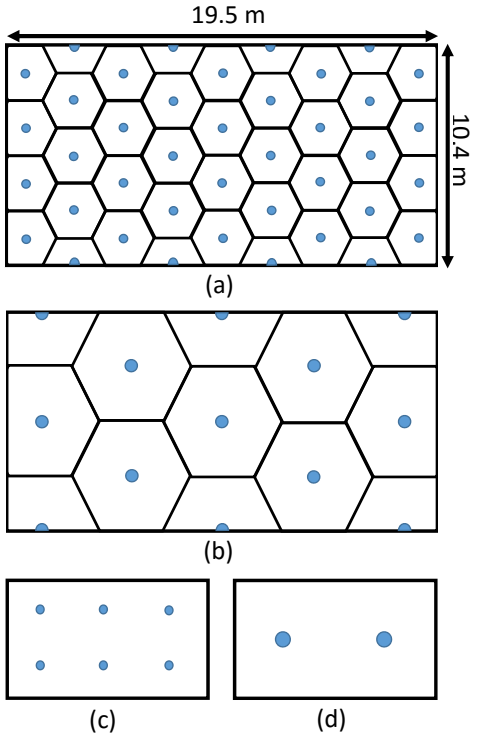

Fig. 2: Layout of single-element and multi-element transmitters in the room: (a) Single-element layout, (b) Each transmitter has 3 LEDs, (c) Each transmitter has 7 LEDs, (d) Each transmitter has 19 LEDs (see Fig. 1). Each configuration has similar total number of LEDs within the room.

• **Scenario-1:** Each individual LED is assumed to transmit a different data stream. This scenario considers rooms where there are large number of VLC receivers, each connected to a different LED. It also captures LEDs which are not used for communication, but still are active to maintain illumination in the room. As a result, the VLC signal from a desired LED will be interfered by a large number of other LEDs.

Based on (11), the power of the received signal can be calculated as

$$P_{\text{rx}} = P_{\text{t}} \times \sum_{d=0}^{\infty} \{\mathbf{p}_d(f)\}_{11}, \tag{14}$$

where P_{t} is the power of the optical signal transmitted by an

LED. Then, the SINR can be expressed as

$$SINR = \frac{(rP_{\mathrm{rx}(v,x)})^2}{\big(\sum_{k=1}^{K}\sum_{m=1}^{M}(rP_{\mathrm{rx}(k,m)})^2\big) - (rP_{\mathrm{rx}(v,x)})^2 + N_0W}, \quad (15)$$

where r is the reflectance factor of receiver's PD, $P_{\mathrm{rx}(k,m)}$ stands for the received signal power from the kth VAP's mth LED, v represents the associated VAP, x represents associated LED, $P_{\mathrm{rx}(v,x)}$ is the received power from the vth VAP's xth LED, M is the number of LEDs on a VAP, K is the total number of VAPs, W denotes the LED modulation bandwidth, and N_0 is the noise power spectral density of ambient noise.

• **Scenario-2:** In Scenario-2 all LEDs at a given transmitter serve to the same user, whereas the LEDs at other transmitters introduce interference. In other words, this scenario assumes that at a given time, there is only one user connected to the set of all LEDs at a given transmitter.

For this scenario, SINR is obtained as

$$SINR = \frac{\big(\sum_{m=1}^{M} rP_{\mathrm{rx}(v,m)}\big)^2}{\sum_{k\neq x}\big(\sum_{m=1}^{M} rP_{\mathrm{rx}(k,m)}\big)^2 + N_0W}, \quad (16)$$

where $P_{\mathrm{rx}(v,m)}$ is the received signal power from the xth VAPs mth LED.

C. Illumination Level Calculation

Calculation of illumination level for a certain location in the room is similar to calculation of communication signal power. Extending the FOV of receiver to π, we can get overall DC gain from an LED to the location of the receiver. Then, based on (11), the illumination level at a certain location is

$$I = P_0\eta \times \sum_{d=0}^{\infty}\{\mathbf{p}_d(f)\}_{11}/A_{\mathrm{R}} \quad (17)$$

where P_0 is the transmit power of an LED as mentioned in Section II , η is luminous efficacy of LED in in lumens per watt $(\mathrm{lm/W})$ and I is the illumination level in lux $[\mathrm{lm/m^2}]$.

V. Simulation Results

Computer simulations are performed to investigate communication and illumination trade-offs for different multi-element transmitter configurations and geometries. In summary there are 40 LEDs for single-element transmitter scenario, 39 LEDs for 3-element transmitter scenario, 42 LEDs for 7-element transmitter scenario, and 38 LEDs for 19-element transmitter scenario. Due to geometrical constraints, it was not possible to use the same exact number of LEDs within the room, and impact on the final results is assumed negligible. For denser topologies (first two scenarios), a hexagonal deployment is considered [8], while for the last two scenarios, transmitters are deployed in a more uniform manner (see Fig. 2).

Vertical tilting of the LEDs and spacing between transmitters for different configurations have been selected heuristically, after testing various different alternatives. For the 3-element transmitter scenario, we have $\alpha = 10°$. For the 7-element transmitter scenario, $\alpha = 20°$, and for the 19-element scenario $\alpha = 17°$, and $\beta = 13°$. Other simulation parameters are shown at Table I and they are the same as in [10]. Interference is considered to be the dominant factor in SINR and impact of additive noise is neglected.

TABLE I: Simulation parameters.

Area of Optival Receiver, A_{R}	400 mm^2
Receiver FOV, θ_{FOV}	40°
Reflectance factor, r	0.5 A/W
Transmitter half-intensity radiation angle, θ_{tx}	25°
Surface half-intensity radiation angle, θ_{surf}	60°
Transmission power of an LED, P_{t}	2.2 W
Power of an LED, P_0	3 W
Modulation Bandwidth, W	20 MHz
AWGN spectral density, N_0	$2.5x10^{-23}$ A/Hz
Luminuous efficacy, η	60 lm/W

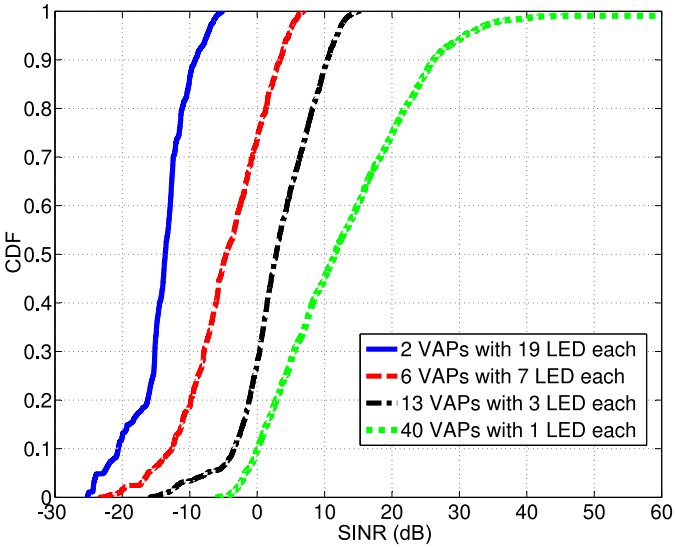

Fig. 3: Empirical CDF of SINR when all LEDs on a VAP transmit a different data (Scenario-1).

As shown in [15], up to four multipath reflections include more than 98 percent of all the light power that receiver can receive. Therefore, we considered generation of four reflections while obtaining multipath signal realizations. Increasing the number of multipath reflections will have limited improvements in simulation accuracy, while it will extensively increase simulation complexity. We assumed the reflection coefficient of the walls, ceiling and floor are 0.8, 0.8, and 0.3, respectively. Transmitters are placed on ceiling pointing downwards and receiver is placed at a height 0.85 m pointing upwards. By changing the place of the receiver at all around the room and estimating achievable SINR, we calculated empirical CDF of SINR.

A. SINR Distributions for Different Configurations

In Fig. 3, CDF of SINR is shown for Scenario-1. As all the other LEDs at a given transmitter are assumed to be interference sources (e.g., since they are serving to different users) this scenario yields low SINR geometries. When the number of LEDs in a VAP increases, SINR decreases dramatically. The reason is, since LEDs are closer to each other at multi-element VAPs, they cause significant interference to each other.

In Fig. 4 CDF of SINR in Scenario-2 is illustrated. In this case, all LEDs that are on the same VAP transmit the same data to the same user. Therefore, LEDs on the same VAP do not cause interference to each other but rather the received

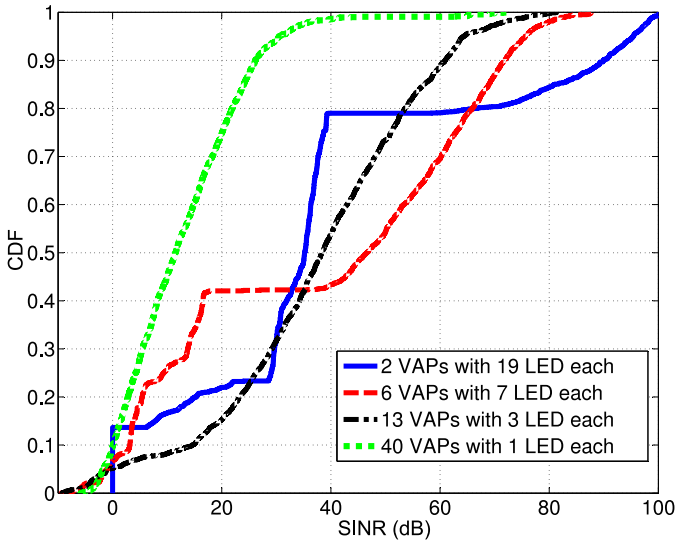

Fig. 4: Empirical CDF of SINR when all LEDs on a VAP transmit the same data (Scenario-2).

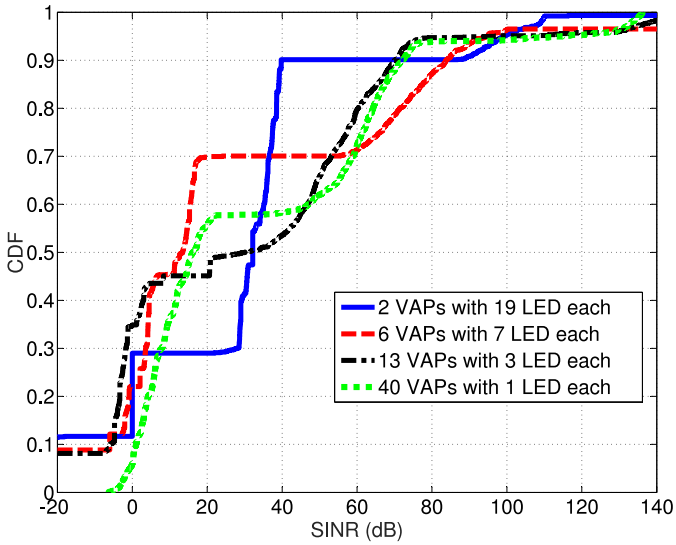

Fig. 5: Empirical CDF of SINR with narrower receiver FOV 30° (Scenario-2).

power at the desired user is improved. Therefore SINR is higher for multi-element VAPs than single-element VAPs. At high SINR region, SINR of VAPs with more LEDs have better SINRs when compared to the VAPs with fewer LEDs. These high SINRs are reached beneath the VAPs, where the received signal strength is strong and interference power is small. For such configurations, the distance between the VAPs is large, which helps to keep interference level low. At 19-element configuration, a step-wise CDF behavior is observed. Around 25% of the locations have SINRs lower than 30 dB, which correspond to the area between the two VAPs. On the other hand, around 20% of the locations have SINRs larger than 70 dBm which correspond to the area directly beneath the VAPs. The configuration with 7 LEDs also shows similar step-wise distribution due to similar reasons.

The CDF of 3-element configuration is smoother than other multi-element scenarios in Fig. 4, which also implies a more uniform coverage distribution in the room. The reason for that is cell sizes of 3 LED VAPs are smaller and there is no sharp transition between coverage areas. In terms of SINR CDFs, all multi-element VAPs are better than single-element VAP. SINR distribution of single-element VAP is the same with that of Scenario-1, and they are technically equivalent.

When comparing two scenarios, we need to mention that Scenario-1 is the worst case scenario in terms of SINR distributions. Since LEDs are assumed to send different data to different users (or, some may simply be utilized for lighting purposes), they cause high interference to each other. This scenario can only be advantageous if there is a large number of users to be supported. For a scenario with large number of users, alternative solutions that include grouping of neighboring LEDs for transmission to same user, or using different transmission powers at different LEDs can also be considered. We have not considered such approaches in this paper and leave them as a future work.

B. Impact of FOV on SINR Distributions

We also investigated effect of FOV on SINR of different transmitter configurations for Scenario-1. In Fig. 5, SINR performance of four different VAPs with a narrower receiver FOV are shown. While in the earlier simulations of Fig. 3 and Fig. 4 the FOV is 40°, in this simulation it is 30°. In this figure in comparison to Fig. 4, single-element VAP shows a better performance, whereas the performance of the other three configurations deteriorate. In the high SINR region, 3-element and 7-element VAPs can achieve SINRs over 100 dB, while around 20% of the locations have SINRs below 0 dB, which implies high outage probability.

The reason for the single-element configuration performing better with narrow receiver FOV is that, since the cell size of single element VAP is smaller, a narrow FOV receiver can take all the signal without taking much interference. With a larger FOV, the VLC receiver observes larger interference from nearby VLC transmitters. However, a lower FOV may also prevent sufficient signal power to be received at the VLC receiver, which may yield catastrophic performance degradations, as can be seen in Fig. 5 for multi-element configurations. In summary, receiver FOV is an important design factor, and it should be taken into account while the separation between the VLC transmitters.

C. Impact of Transmission Power on SINR Distribution

Using VLC with dimmable light sources is recently becoming a popular research topic. Since VLC should also be able to operate in dark environments, it is important that it can be used with low lighting levels. We also investigated performance of four multi-element configurations considering a dimming scenario. In Fig. 6, SINR distribution with very low transmission power is shown. In this simulation, transmission power of an LED P_t is taken as 0.01 W, whereas in Fig. 4 it is taken as 2.2 W. In Fig. 6, noise power is also taken into account. We can see that 7-element and 19-element configurations are more vulnerable to dimming effects, since 30% and 40% of the locations, respectively, observe SINRs below 0 dB. Due to a better outage rate, configurations with 3-LEDs and single LED are more robust to dimming effects. The reason for that is, since cell sizes of these two configurations

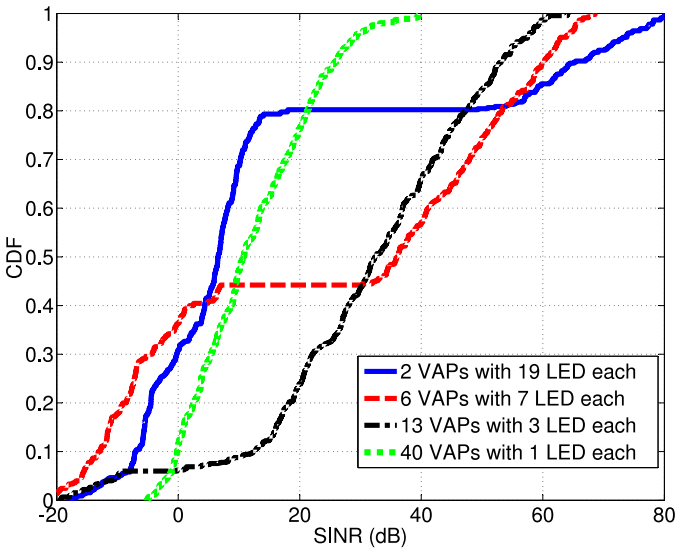

Fig. 6: Empirical CDF of SINR with low transmit power of 0.01 W (Scenario-2).

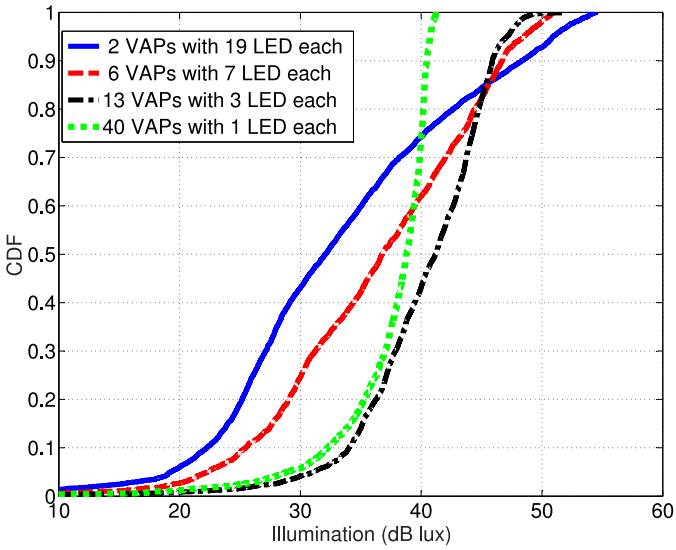

Fig. 7: Empirical CDF of illumination level in the room in dB (same for both scenarios.)

are small, path loss effects are less critical. In general, 3-element VAP gives the best overall SINR distribution, since it is nearly 20 dB higher than single-element configuration in most SINR regions.

D. Illumination Distribution for Different Configurations

Maintaining overall high illumination and even distribution in the room is a critical issue for lighting systems. In Fig. 7, we compare the illumination distributions of the four different multi-element configurations. Single-element VAP configuration yields the most uniform distribution of illumination level within the room. This result is expected, as each LED is mounted uniformly at different location in the room. When number of LEDs on a VAP increased, illumination gets a more heterogeneous nature. When comparing the overall illumination level, 3-element VAP gives a better performance, although it has 1 LED less in comparison with the single-element case. While this might sound surprising, the reason for this behavior is that since the LEDs in the 3-element VAP are mounted with certain tilt from the vertical axis, they make use of wall reflections better. The 7-element VAP and 19-element VAP on the other hand do not provide as even illuminance as others, and this is the result of highly directional LEDs which are only mounted at few locations within the room.

VI. Conclusion

In this paper, we introduced a multi-element VLC transmitter structure and analyzed different configurations' SINR and illumination performance. Effects of FOV and dimming on the SINR distributions are also studied. Our results show that compared to other configurations, a multi-element transmitter architecture with 3 LEDs may provide a good trade-off between illumination and communication, and is also robust against dimming effects. Our future study includes investigation of illumination and communication trade-offs considering the use of multi-element receivers.

References

[1] H. Burchardt, N. Serafimovski, D. Tsonev, S. Videv, and H. Haas, "VLC: Beyond point-to-point communication," *IEEE Commun. Mag.*, vol. 52, no. 7, pp. 98–105, July 2014.

[2] A. Sevincer, A. Bhattarai, M. Bilgi, M. Yuksel, and N. Pala, "LIGHTNETs: smart lighting and mobile optical wireless networks – a survey," *IEEE Commun. Surveys and Tutorials*, vol. 15, no. 4, Apr. 2013.

[3] Y. S. Eroglu, I. Guvenc, N. Pala, and M. Yuksel, "AOA-based localization and tracking in multi-element VLC systems," in *Proc. IEEE Wireless and Microwave Technology Coneference (WAMICON)*, Apr. 2015.

[4] A. Sahin, Y. S. Eroglu, I. Guvenc, N. Pala, and M. Yuksel, "Accuracy of AOA-based and RSS-based 3D localization for visible light communications," in *Proc. IEEE Vehic. Technol. Conf. (VTC)*, Boston, MA, Sep. 2015.

[5] S. Rajagopal, R. Roberts, and S.-K. Lim, "IEEE 802.15.7 visible light communication: modulation schemes and dimming support," *IEEE Commun. Mag.*, vol. 50, no. 3, pp. 72–82, Mar. 2012.

[6] H. Sugiyama, S. Haruyama, and M. Nakagawa, "Brightness control methods for illumination and visible-light communication systems," in *Proc. IEEE Int. Conf. Wireless and Mobile Commun. . (ICWMC)*, Mar. 2007, pp. 78–78.

[7] A. Tsiatmas, C. Baggen, F. Willems, J.-P. Linnartz, and J. Bergmans, "An illumination perspective on visible light communications," *IEEE Commun. Mag.*, vol. 52, no. 7, pp. 64–71, July 2014.

[8] J.-H. Liu, Q. Li, and X.-Y. Zhang, "Cellular coverage optimization for indoor visible light communication and illumination networks," *J. Commun.*, vol. 9, no. 11, 2014.

[9] C. Gong and Z. Xu, "Linear receivers for optical wireless scattering communication with multiple photon detectors," in *Globecom Workshops (GC Wkshps)*, Dec. 2014, pp. 438–443.

[10] Z. Chen, D. Tsonev, and H. Haas, "Improving SINR in indoor cellular visible light communication networks," in *Proc. IEEE Int. Conf. Commun. (ICC)*, June 2014, pp. 3383–3388.

[11] A. Nuwanpriya, S.-W. Ho, and C. S. Chen, "Angle diversity receiver for indoor MIMO visible light communications," in *Proc. IEEE Globecom Workshops (GC Wkshps)*, Dec. 2014, pp. 444–449.

[12] A. Tsiatmas, F. Willems, and S. Baggen, "Optimum diversity combining techniques for visible light communication systems," in *Globecom Workshops (GC Wkshps)*, Dec. 2014, pp. 456–461.

[13] P. Palathingal, I. Guvenc, N. Pala, and M. Yuksel, "A multi-element vlc architecture for high spatial reuse," in *ACM Workshop on Visible Light Communication Systems*, 2015.

[14] J. Barry, J. Kahn, W. Krause, E. Lee, and D. Messerschmitt, "Simulation of multipath impulse response for indoor wireless optical channels," *IEEE J. Select. Areas Commun. (JSAC)*, vol. 11, no. 3, pp. 367–379, Apr. 1993.

[15] Y. Alqudah and M. Kavehrad, "Mimo characterization of indoor wireless optical link using a diffuse-transmission configuration," *IEEE Trans. Commun.*, vol. 51, no. 9, pp. 1554–1560, Sep. 2003.